Further reading

- *Introduction to Texture Analysis: Macrotexture, Microtexture and Orientation Mapping*, Valerie Randle and Olaf Engler (2000) Taylor & Francis; ISBN 9056992244
- *Electron Backscatter Diffraction in Materials Science*, Eds Adam J Schwartz, Mukul Kumar, Brent L Adams (2000) Kluwer Academic; ISBN 0-306-46487-X

Visit the Oxford Instruments EBSD website at www.ebsd.com

PATENTS
EP 0325383
EP 0302716
US 4931650
GB 2192091
US 5170229
US 5357110
JP 2557692
JP 2581597
EU 0568351

CERTIFICATE NUMBER FM29142

Printed in England.

Ref: OIA/092/A/0304

Oxford Instruments Analytical

UK
Halifax Road, High Wycombe
Bucks, HP12 3SE England
Tel: +44 (0) 1494 442255
Fax: +44 (0) 1494 461033
Email: analytical@oxinst.co.uk

Australia
Sydney, N.S.W. 1715
Tel: +61 2 9484 6108
Fax: +61 2 9484 1667
Email: sales@oxinst.com.au

China
Beijing
Tel: +86 (10) 6518 8160/1/2
Fax: +86 (10) 6518 8155
Email: info@oxford-instruments.com.cn

France
Saclay, Cedex
Tel: +33 (0) 1 69 85 25 24
Fax: +33 (0) 1 69 41 86 80
Email: analytical-info@oxford-instruments.fr

Germany
Wiesbaden
Tel: +49 (0) 6122 937 176
Fax: +49 (0) 6122 937 178
Email: analytical@oxford.de

Japan
Tokyo
Tel: +81 (0) 3 5245 3591
Fax: +81 (0) 3 5245 4466/4477
Email: oikkma@oxinst.co.jp

Latin America
Clearwater FL
Tel: +1 727 538 7702
Fax +1 727 538 4205
Email: oxford@gate.net

Scandinavia
Link Nordiska AB
Lidingö, Sweden
Tel: +46 8 590 725 50
Fax: +46 8 590 725 58
Email: info@linknord.se
Web: www.linknord.se

Singapore
Tel: +65 6337 6848
Fax: +65 6337 6286
Email:
analytical.sales@oxford-instruments.com.sg

USA
Concord MA
Tel: +1 978 369 9933
Toll Free: +1 800 447 4717
Fax: +1 978 369 8287
Email: info@ma.oxinst.com

www.oxford-instruments.com

Oxford Instruments Analytical – **technical briefing**

Electron Backscattered Diffraction

Explained

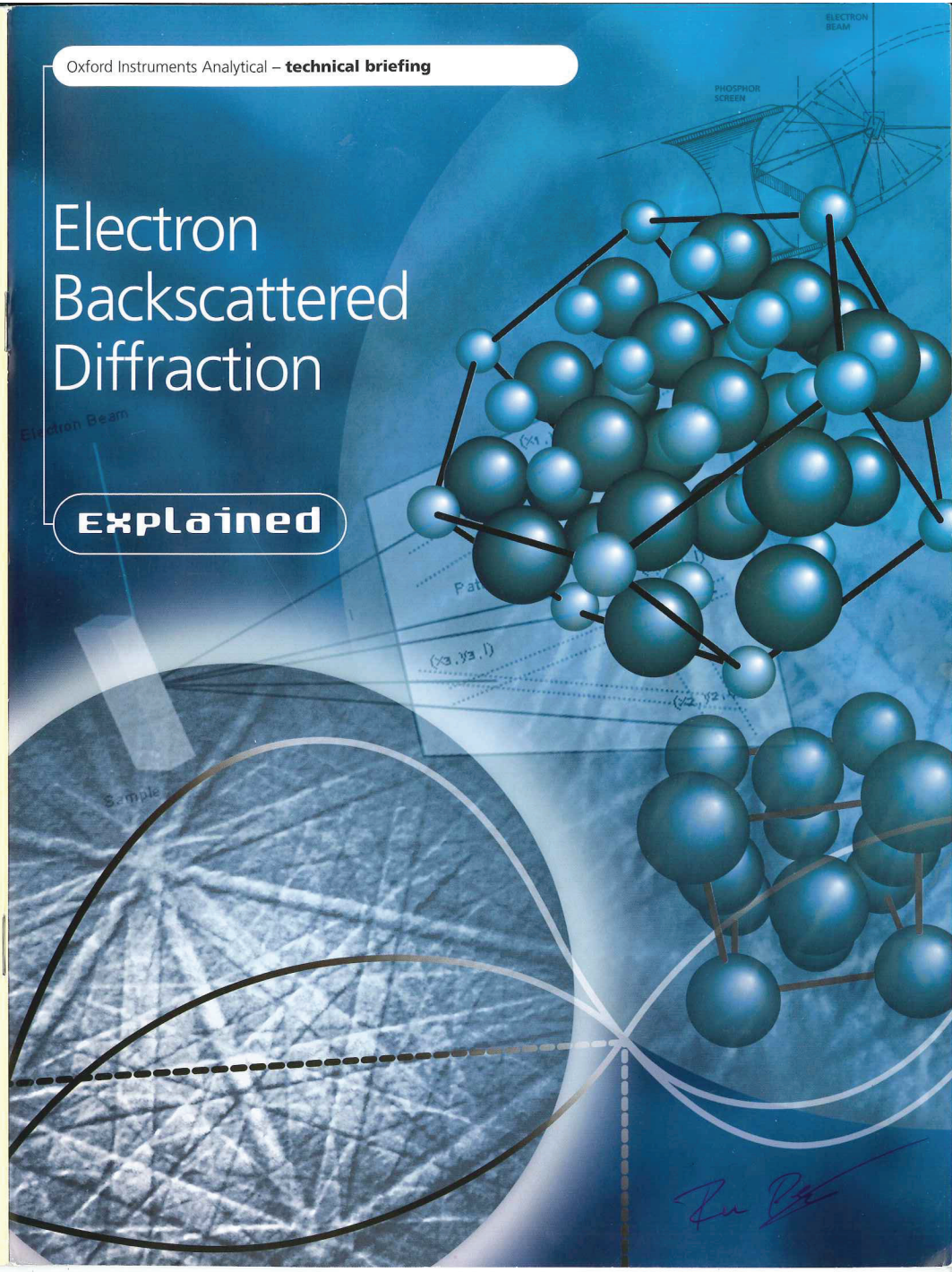

Contents

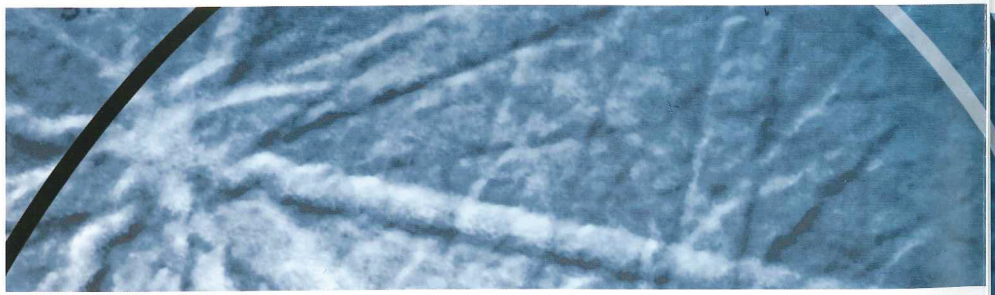

Introduction

Electron Backscattered Diffraction (EBSD) is a technique which allows crystallographic information to be obtained from samples in the scanning electron microscope (SEM). In EBSD a stationary electron beam strikes a tilted crystalline sample and the diffracted electrons form a pattern on a fluorescent screen. This pattern is characteristic of the crystal structure and orientation of the sample region from which it was generated. The diffraction pattern can be used to measure the crystal orientation, measure grain boundary misorientations, discriminate between different materials, and provide information about local crystalline perfection. When the beam is scanned in a grid across a polycrystalline sample and the crystal orientation measured at each point, the resulting map will reveal the constituent grain morphology, orientations, and boundaries. This data can also be used to show the preferred crystal orientations (texture) present in the material. A complete and quantitative representation of the sample microstructure can be established with EBSD.

In the last ten years EBSD has become a well established technique for the SEM, and obtaining crystallographic information from samples is now both routine and easy. This guide explains how an EBSD system works, describes the experiments that can be performed and how to undertake them, and finally outlines the basic crystallography needed for EBSD.

Section 1

Basics of EBSD

Principal system components

The principal components of an EBSD system are (Figure 1):

- A sample tilted at 70° from the horizontal.
- A phosphor screen which is fluoresced by electrons from the sample to form the diffraction pattern.
- A sensitive charge coupled device (CCD) video camera for viewing the diffraction pattern on the phosphor screen.
- A vacuum interface for mounting the phosphor and camera in an SEM port. The camera monitors the phosphor through a lead glass screen in the interface, and the phosphor can be retracted to the edge of the SEM chamber when not in use.
- Electronic hardware that controls the SEM, including the beam position, stage, focus, and magnification.
- A computer to control EBSD experiments, analyze the diffraction pattern and process and display the results.
- An optional electron detector mounted below the phosphor screen for electrons scattered in the forward direction from the sample.

Figure 1: Components of an EBSD system

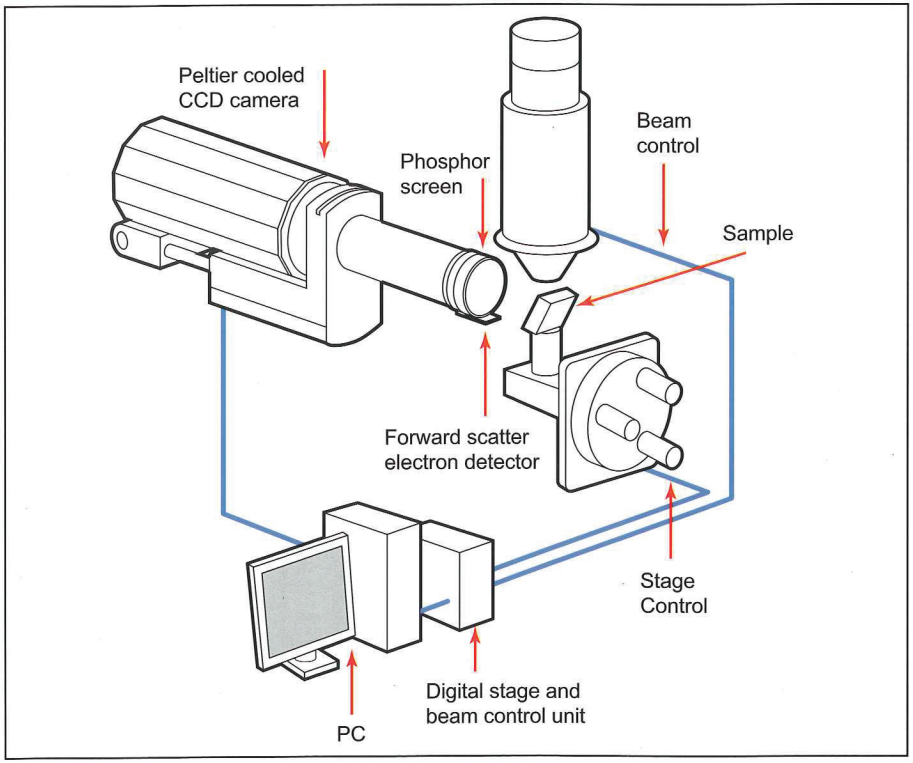

Pattern formation and collection

For EBSD, a beam of electrons is directed at a point of interest on a tilted crystalline sample in the SEM (Figure 2). The mechanism by which the diffraction patterns are formed is complex, but the following model describes the principal features. The atoms in the material inelastically scatter a fraction of the electrons, with a small loss of energy, to form a divergent source of electrons close to the surface of the sample. Some of these electrons are incident on atomic planes at angles which satisfy the Bragg equation:

$$n\lambda = 2d \sin \theta \qquad (1)$$

where n is an integer, λ is the wavelength of the electrons, d is the spacing of the diffracting plane, and θ is the angle of incidence of the electrons on the diffracting plane. These electrons are diffracted to form a set of paired large angle cones corresponding to each diffracting plane. When used to form an image on the fluorescent screen, the regions of enhanced electron intensity between the cones produce the characteristic Kikuchi bands of the electron back scattered diffraction pattern (Figure 3).

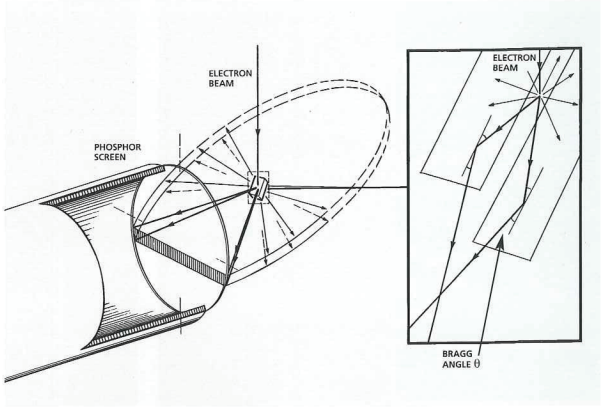

Figure 2: Formation of the diffraction pattern

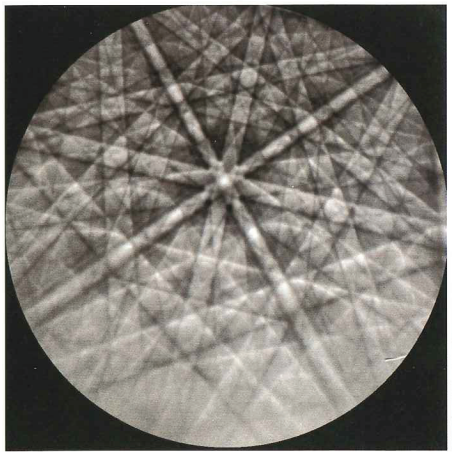

Figure 3: A diffraction pattern from nickel collected at 20 kV accelerating voltage

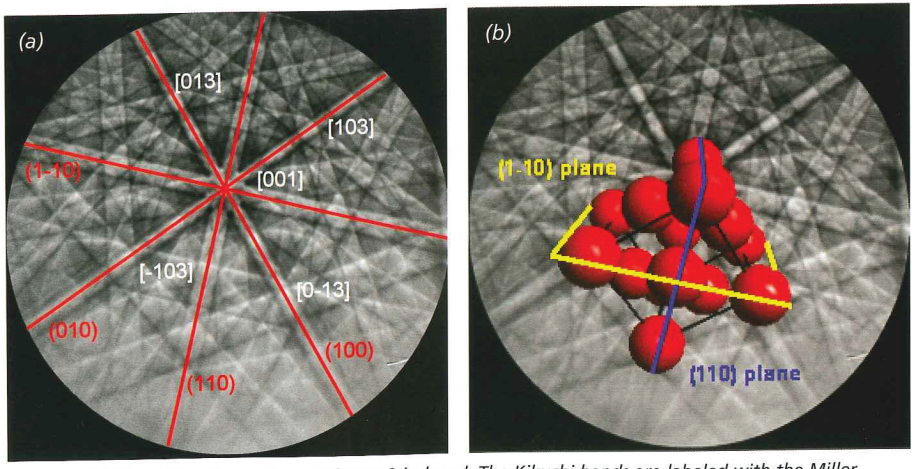

Figure 4: (a) The diffraction pattern in figure 3 indexed. The Kikuchi bands are labeled with the Miller indices of the crystal planes that formed them (red) and the crossing points of the bands are labeled with the zone axis symbol (white). (b) The nickel unit cell orientation which generates this pattern with the corresponding crystal planes shown.

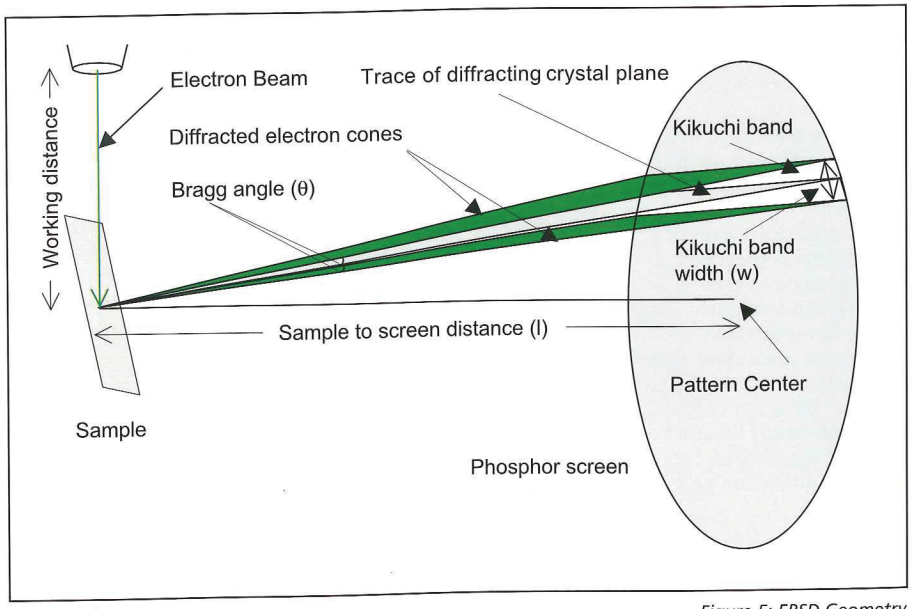

Figure 5: EBSD Geometry

Interpreting diffraction patterns

The center lines of the Kikuchi bands correspond to the intersection of the diffracting planes with the phosphor screen. Hence, each Kikuchi band can be indexed by the Miller indices of the diffracting crystal plane which formed it. The intersections of the Kikuchi bands correspond to zone axes in the crystal and can be labeled by zone axis symbols (Figure 4).

The semi-angle of the diffracted cones of electrons is (90 - θ) degrees. For EBSD this is a large angle so the Kikuchi bands approximate to straight lines. For example, the wavelength of 20 kV electrons is 0.00859 nm and the spacing of the (111) plane in aluminum is 0.233 nm making the cone semi-angle 88.9°.

The width w of the Kikuchi bands close to the pattern center is given by:

$$w \approx 2l\theta \approx \frac{nl\lambda}{d} \qquad (2)$$

where l is the distance from the sample to the screen (Figure 5). Hence, planes with wide d-spacings give thinner Kikuchi bands than narrow planes. Because the diffraction pattern is bound to the crystal structure of the sample, as the crystal orientation changes the resultant diffraction pattern also changes. The positions of the Kikuchi bands can therefore be used to calculate the orientation of the diffracting crystal (Figure 6).

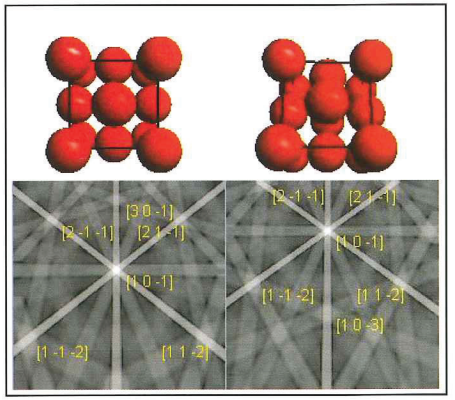

Figure 6: Changes in the crystal orientation result in movement of the diffraction pattern. The simulated diffraction pattern is from a sample tilted 70° to the horizontal and the crystal orientation is viewed along the direction perpendicular to the sample.

Calibrating the EBSD system

EBSD system calibration measures the sample to screen distance and the pattern center position on the phosphor screen (Figure 5). The pattern center is the point on the screen closest to the generation point of the diffraction pattern on the sample. There are several methods for calibrating an EBSD system.

One method to measure the pattern center position is to collect a diffraction pattern with the screen both in the normal and partly retracted position and to measure the positions of the same zone axes on both patterns (Figure 7).

The screen to sample distance is calculated by measuring the distance between two zones separated by a known angle with the screen in the operating position. The calibration can also be performed using a single pattern by iteratively fitting the pattern center and sample to screen distance to minimize the error in the orientation measurement.

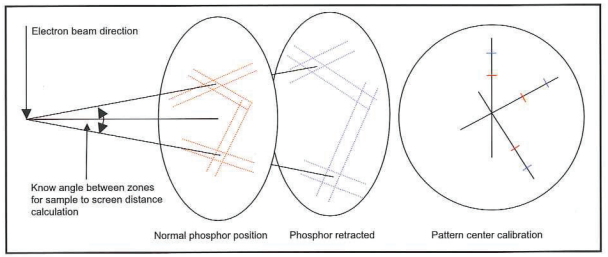

Figure 7: EBSD system calibration. Lines joining the position of the same features on the phosphor in the normal and retracted position meet at the pattern center.

Automated indexing and orientation measurement

The crystal orientation is calculated from the Kikuchi band positions by the computer processing the digitized diffraction pattern collected by the CCD camera. The Kikuchi band positions are found using the Hough transform. The transform between the coordinates (x, y) of the diffraction pattern and the coordinates (ρ, θ) of Hough space is given by (Figure 8):

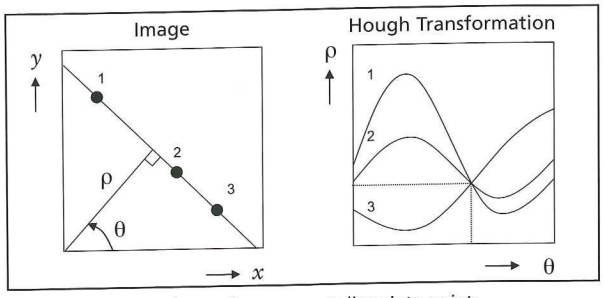

Figure 8: The Hough transform converts lines into points in Hough space

$$\rho = x \cos\theta + y \sin\theta \qquad (3)$$

A straight line is characterized by ρ, the perpendicular distance from the origin and θ the angle made with the x-axis and so is represented by a single point (ρ, θ) in Hough space. Kikuchi bands transform to bright regions in Hough space which can be detected and used to calculate the original positions of the bands (Figure 9).

Figure 9: Finding the position of the Kikuchi bands in the diffraction pattern using the Hough transform

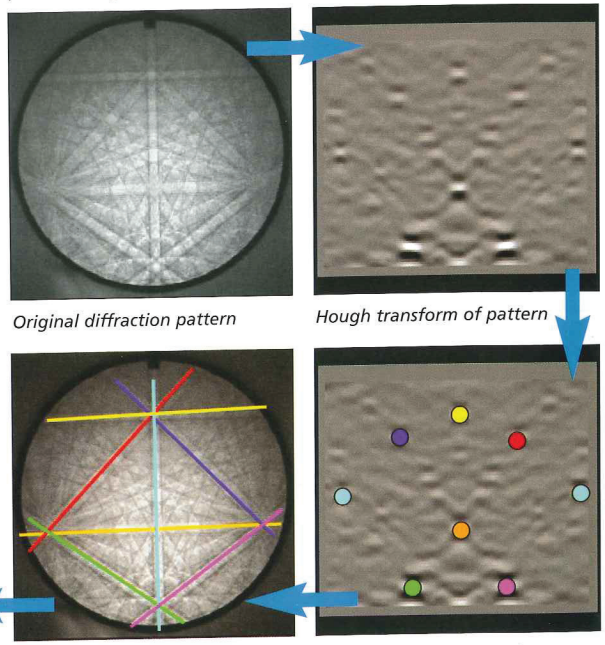

Original diffraction pattern

Hough transform of pattern

Indexed diffraction pattern

Corresponding Kikuchi bands found on diffraction pattern

Detected peaks in Hough transform

Using the system calibration, the angles between the planes producing the detected Kikuchi bands can be calculated (Box 1). These are compared with a list of inter-planar angles for the analyzed crystal structure to allocate Miller indices to each plane. The final step is to calculate the orientation of the crystal lattice with respect to coordinates fixed in the sample (Box 2). This whole process takes less than a few milliseconds with modern computers.

Box 1: Calculating the angle between crystal planes from measurements on the diffraction pattern

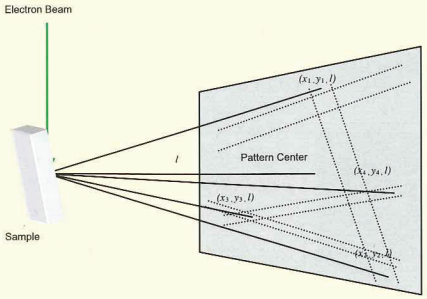

Two Kikuchi bands are defined by the pairs of points $(x_1\ y_1 l)$, $(x_2\ y_2 l)$ and $(x_3\ y_3 l)$, $(x_4\ y_4 l)$.

The vector $\mathbf{r}_i$ joins the point of incidence of the electron beam on the sample to the point $(x_i\ y_i l)$.

The unit vector $\mathbf{n}_1 = \mathbf{r}_1 \times \mathbf{r}_2 / |\mathbf{r}_1 \times \mathbf{r}_2|$ is perpendicular to the crystal plane generating the first Kikuchi band and the vector $\mathbf{n}_2 = \mathbf{r}_3 \times \mathbf{r}_4 / |\mathbf{r}_3 \times \mathbf{r}_4|$ is perpendicular to the crystal plane generating the second Kikuchi band.

The angle between the planes forming the two Kikuchi bands is $\cos^{-1}(|\mathbf{n}_1 \bullet \mathbf{n}_2|)$

Box 2: Representing crystal orientations

A common method for representing a crystal orientation is to use the ideal orientation nomenclature (hkl)[uvw]. Directions in the crystal are referred to a set of coordinates fixed in the sample. Using the terminology of rolled sheet metals, these are the sample normal (ND), rolling direction (RD) and transverse direction (TD). In the ideal orientation nomenclature the normal to the crystal plane (hkl) is parallel to the sample normal and the crystal direction [uvw] parallel to the rolling direction (Figure 10). The notation {hkl}<uvw> denotes the symmetrically related set of directions which represent the texture.

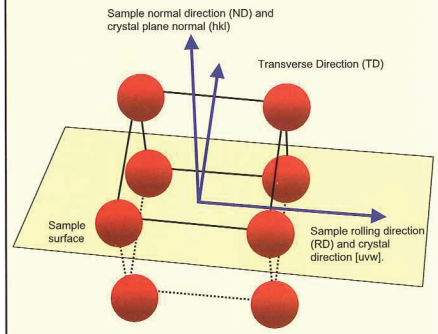

Figure 10: Meaning of ideal orientation nomenclature (hkl)[uvw]. Here the (110) plane normal is parallel to the normal direction and the [001] direction is parallel to the rolling direction, so the texture is (110)[001]

The orientation in figure 10 can also be represented by three Euler angles $\varphi_1 \Phi \varphi_2$ (see section 3) with φ_1=135°, Φ=90° and φ_2=90°.

Band intensity

The mechanisms giving rise to the Kikuchi band intensities and profile shapes are complex. As an approximation, the intensity of a Kikuchi band I_{hkl} for the (hkl) plane is given by:

$$I_{hkl} = \left[\sum_i f_i(\theta) \cos 2\pi (hx_i + ky_i + lz_i)\right]^2 + \left[\sum_i f_i(\theta) \sin 2\pi (hx_i + ky_i + lz_i)\right]^2 \quad (4)$$

where $f_i(\theta)$ is the atomic scattering factor for electrons and $(x_i\ y_i\ z_i)$ are the fractional coordinates in the unit cell for atom i. An observed diffraction pattern should be compared with a simulation calculated using equation 4, to ensure only planes that produce visible Kikuchi bands are used when solving the diffraction pattern (Figure 11). This is especially important when working with materials with more than one atom type.

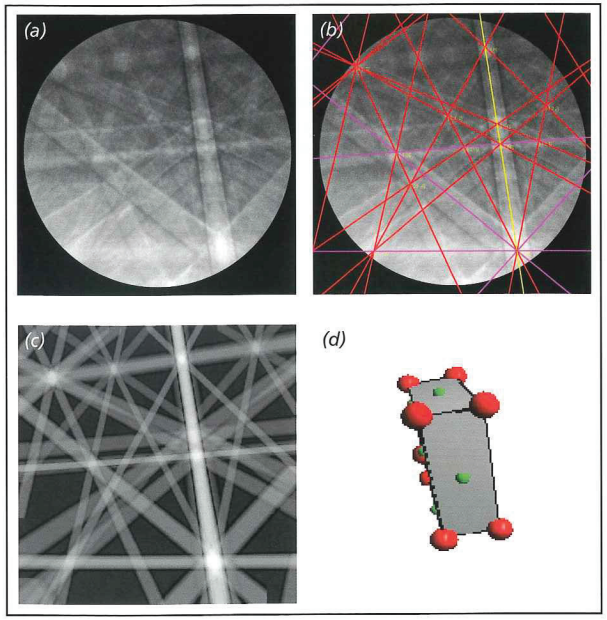

Figure 11: Diffraction pattern band intensities.

(a) Diffraction pattern from the orthorhombic ceramic mullite ($3Al_2O_3\ 2SiO_2$) collected at 10 kV accelerating voltage.

(b) Solution overlaid on the diffraction pattern giving the crystal orientation as {370}<7-34>

(c) Simulated diffraction pattern showing all Kikuchi bands with intensity greater than 10% of the most intense band.

(d) Simulation of crystal orientation giving the solution shown in (b).

Summary

- When an electron beam is incident on a tilted crystalline sample, electron backscatter diffraction patterns are formed on a suitably placed phosphor screen.
- The diffraction pattern consists of a set of Kikuchi bands which are characteristic of the sample crystal structure and orientation.
- The center line of each Kikuchi band corresponds to the intersection with the phosphor screen of the diffracting plane responsible for the band.
- The position of the Kikuchi bands can be found automatically with the Hough transform and used to calculate the crystal orientation of the sample region that formed the pattern.

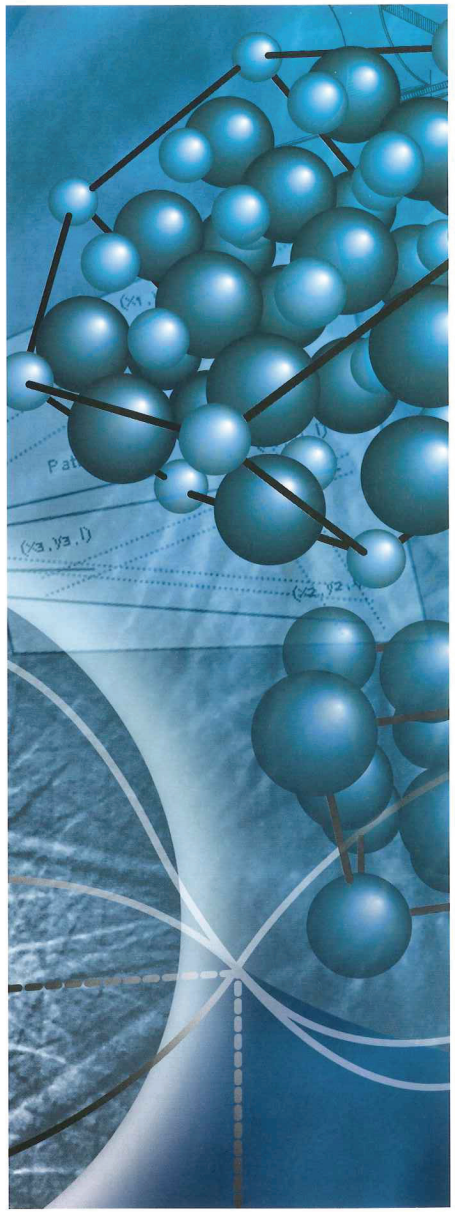

Section 2

Types of EBSD experiment

Point analysis

In EBSD point analysis the beam is positioned at a point of interest on the sample, a diffraction pattern collected and the crystal orientation calculated. This provides a quick overview of the crystallinity of the sample and the range of grain orientations present (Figure 12).

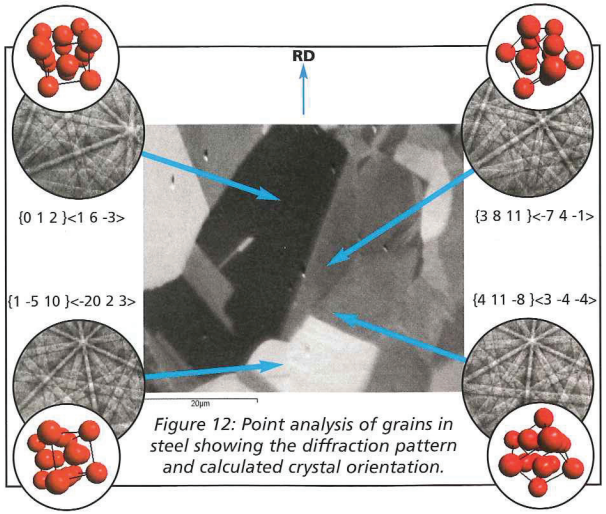

Figure 12: Point analysis of grains in steel showing the diffraction pattern and calculated crystal orientation.

Crystal Orientation Mapping

In crystal orientation mapping, the electron beam is scanned over the sample on a grid of points and at each point a diffraction pattern obtained and the crystal orientation measured. The resulting data can be displayed as a crystal orientation map and processed to provide a wide variety of information about the sample microstructure (Figure 13). Large sample areas can be measured by automatically moving the SEM stage between successive maps.

The maps shown are based on the sample normal, rolling and transverse directions. At each point in the map, the crystallographic direction corresponding to the particular sample direction is calculated, and a color allocated according to its position in the inverse pole figure. (Figure 14)

Figure 13: Crystal orientation maps from austenitic stainless steel collected at 20 kV accelerating voltage. The map step size is 0.72 µm and contains 49152 crystal orientation measurements.

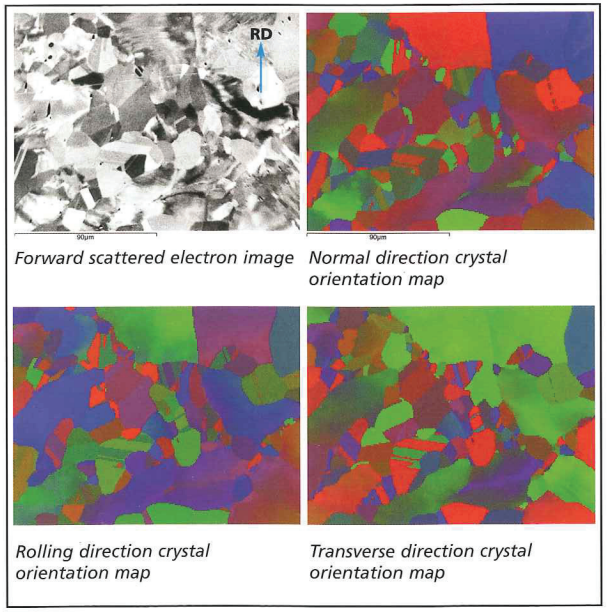

Forward scattered electron image

Normal direction crystal orientation map

Rolling direction crystal orientation map

Transverse direction crystal orientation map

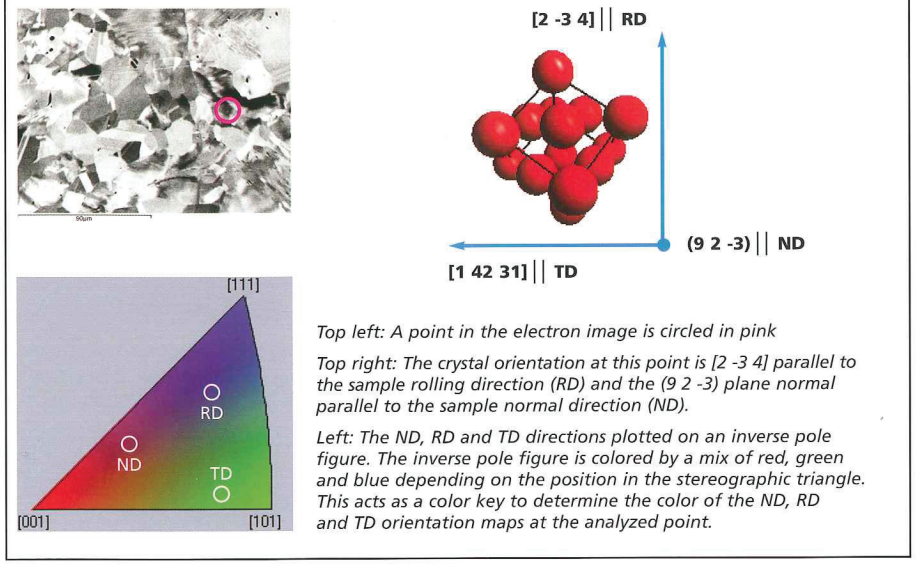

Top left: A point in the electron image is circled in pink

Top right: The crystal orientation at this point is [2 -3 4] parallel to the sample rolling direction (RD) and the (9 2 -3) plane normal parallel to the sample normal direction (ND).

Left: The ND, RD and TD directions plotted on an inverse pole figure. The inverse pole figure is colored by a mix of red, green and blue depending on the position in the stereographic triangle. This acts as a color key to determine the color of the ND, RD and TD orientation maps at the analyzed point.

Figure 14: Coloring of crystal orientation maps

Pattern quality maps

The diffuseness or quality of the diffraction pattern is influenced by a number of factors including local crystalline perfection, sample preparation, surface contamination and the phase and orientation being analyzed.

The height of the peaks in the Hough transform gives a measure of the pattern quality. One algorithm for calculating pattern quality p is:

$$p = \sum_{i=1\text{-}3} h_i / 3\sigma_h \qquad (5)$$

where h_i is the peak height of the Hough transform of the ith most intense Kikuchi band and σ_h is the standard deviation of the Hough transform. Pattern quality maps will often reveal features invisible in the electron image such as grains, grain boundaries and surface damage such as scratches (Figure 15).

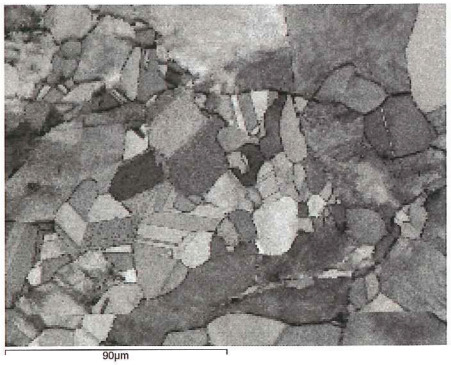

Figure 15: Pattern quality map from sample shown in Figure 13.

Representation o
and grain bound

Unlike an optical or scan
must reveal the positions
microstructure (Figure 17
the collection of neighbo
less than a certain thresh
from the data collected fo
boundary misorientation
grain boundaries can be s

Box 3: Grains and gr

Many materials are form
of the interface between
of the bulk material. Gra
and the boundary plane.
presence in a material m
of sites on either side of
are characterized by Σ, v
cell. Two examples of spe

Figure 16: Special grain bo

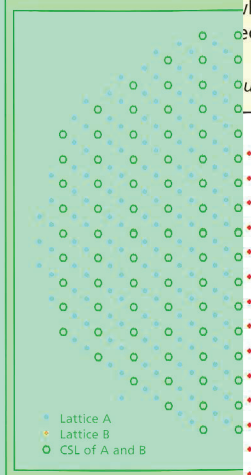

The Σ3 boundary (twin boundary) is a 36.9° rotatio about the [111] direction.

f grains
aries

ing electron micrograph, the crystal orientation map
of all grains and grain boundaries in the sample
. In crystal orientation mapping a grain is defined by
uring pixels in the map, which have a misorientation
ld angle. The distribution of grain sizes can be measured
r the map. In addition, the distribution of grain
angles and the distribution and position of special
hown (See box 3).

ain boundaries

ed of an aggregate of variously oriented crystals or grains. The nature
the grains, or grain boundaries, can influence the physical properties
in boundaries are characterized by the misorientation axis and angle
Some boundaries satisfy certain geometrical criteria and their
ay confer particular properties. When crystal lattices share a fraction
a grain boundary, they are termed coincident site lattices (CSL). CSL's
here Σ is the ratio of the size of the CSL unit cell to the standard unit
ecial boundaries are shown in Figure 16.

undaries

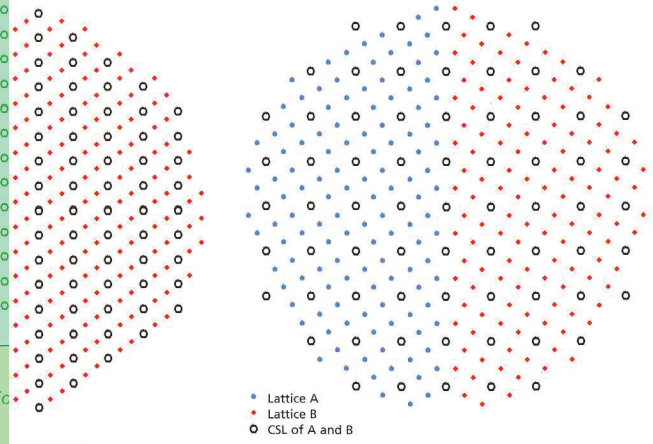

The Σ5 boundary is a 36.9° rotation about the [100] direction.

Figure 17: Grain boundary data measured by EBSD from the sample in Figure 13.

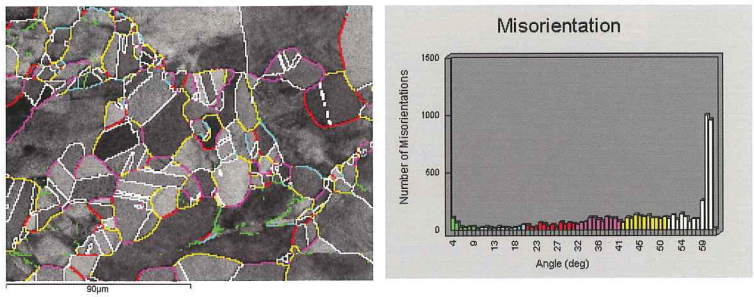

Grain boundary positions superimposed on the pattern quality image (left). The boundaries are color coded according to the histogram of misorientation angle (right). Only boundaries with a misorientation of greater than 3.5° are shown.

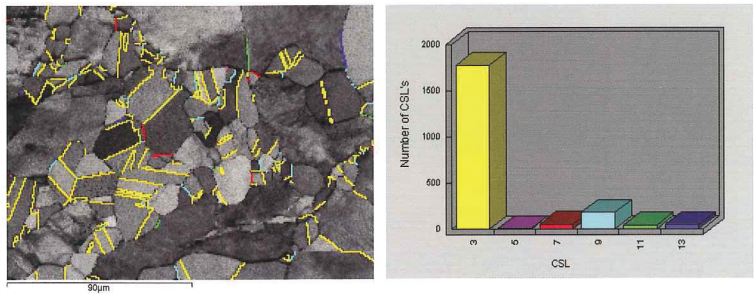

Coincident site lattice (CSL) boundary positions superimposed on the pattern quality image (left). The boundaries are color coded by CSL type shown in the histogram of CSL (right).

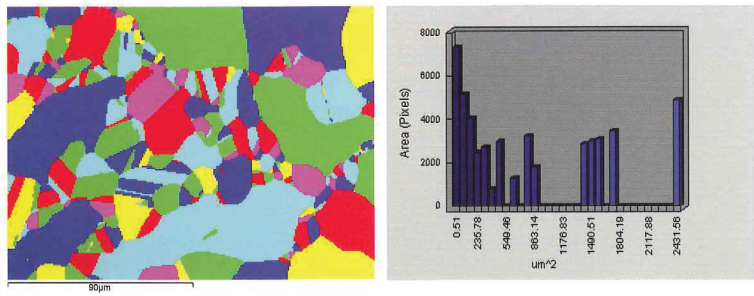

Map showing grain positions (left) and histogram of grain sizes (right). All neighbouring points within a grain have a misorientation less than 3°.

Sample normal direction.

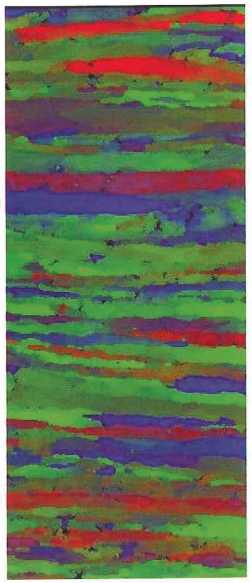

Sample rolling direction.

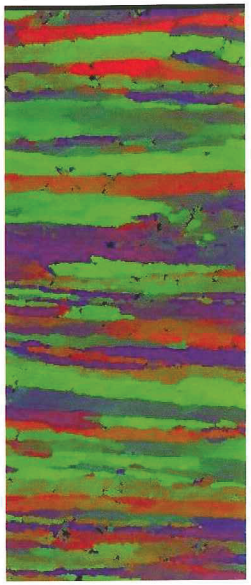

Sample transverse direction.

Individual crystal orientations plotted as an (001) pole figure.

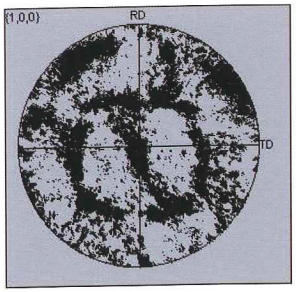

The same data plotted as an (110) pole figure using color contours showing the strength of the texture compared to a random texture.

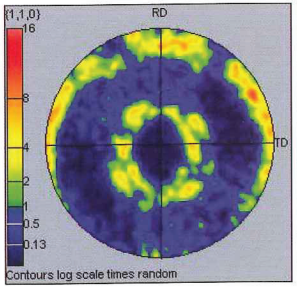

The same data shown as φ_1 φ_2 sections through Euler space at 10° intervals of Φ with the texture strength shown as color contours.

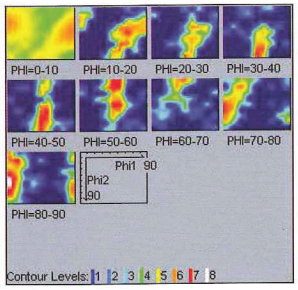

Figure 18: Crystal orientation maps and texture plots from IF steel. The map step size is 51 nm and it contains 109,944 points.

Texture

The individual crystal orientation measurements collected by crystal orientation mapping can be used to show the crystallographic textures developed in the sample (See Box 4). Figure 18 shows a crystal orientation map from a sample of deformed interstitial free (IF) steel together with pole figure and Euler space plots of the individual crystal orientations. The various textures in the sample can be separated automatically, their volume fractions calculated, and the regions of the sample from which they originate shown. This is illustrated in Figure 19 which shows two texture components separated from the map in Figure 18.

Figure 19: Two texture components separated from the data shown in Figure 18 and maps showing where the components originate in the sample.

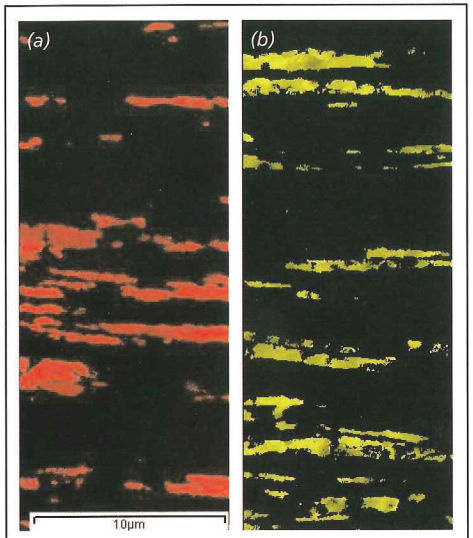

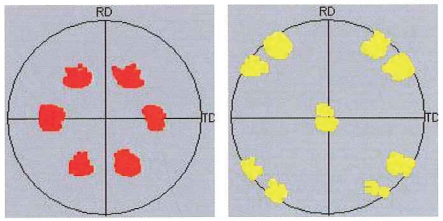

Top left and right:
Regions of sample contributing to extracted texture.

Bottom left and right:
(001) pole figure showing extracted texture. The intensity of the color shows how close the orientation is to the extracted texture.

(a) {8 7 9}<-11 1 9> texture. 13.17% of orientations are within 6° of this texture.

(b) {2 -34 5}<11 3 16> texture. 12.79% of orientations are within 6° of this texture.

Box 4: Preferred orientation and texture

Grains are seldom oriented randomly in polycrystalline materials. The preferred crystallographic orientation or texture of polycrystalline materials influences many properties of the bulk material, because physical properties are often anisotropic with respect to crystal direction. Material processing methods are frequently deliberately chosen to produce certain desired textures. Textures are usually specified by the ideal orientation nomenclature {hkl}<uvw>.

The texture can be represented as a stereographic projection (pole figure) of the directions of selected crystal plane normals (poles). The orientation distribution close to a particular texture will appear as a cluster of points on the pole figure. Textures can also be plotted as a three dimensional plot of the three Euler angles $\varphi_1 \Phi \varphi_2$ (see section 3) associated with each orientation measurement. This is usually presented as a series of two dimensional slices through the Euler space to produce density maps of Euler angles (Figure 20).

Texture is usually measured by X-ray diffraction. The X-ray intensity from a particular diffracting plane is measured, while the sample is stepped through a series of orientations to complete the pole figure. The individual crystal orientations measured with EBSD can also be displayed as pole figures for preferred orientation analysis. The spatial resolution and positioning limitations of X-ray diffraction make EBSD the preferred technique for examining texture on a microscopic scale. However, advances in EBSD processing speed can make the technique competitive with X-ray diffraction for texture measurements from large samples. EBSD and X-ray diffraction are complementary techniques for texture analysis.

Figure 20: Representations of texture.

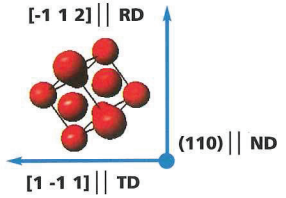

Left: A face centered cubic crystal in the Brass texture orientation {110}<-1 1 2>

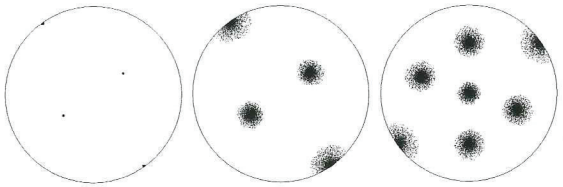

Left: An (001) pole figure for a crystal in the Brass texture orientation.
Middle: A simulated (001) pole figure for the Brass texture drawn as individual orientation points plotted randomly within 15° of the texture.
Right: A simulated (110) pole figure for the Brass texture as individual orientation points plotted randomly within 15° of the texture.

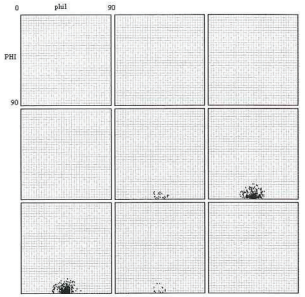

Left: An Euler space plot for the Brass texture. This is shown as individual orientation points plotted randomly within 15° of the texture plotted as the corresponding Euler angles. It is plotted as sections through the three dimensional Euler space. Nine Φ, φ_1 sections are plotted at 10° intervals of φ_2. It shows a cluster of points corresponding to the Euler angles:
$\varphi_1 = 45° \Phi = 90° \varphi_2 = 54.7°$,
which represents the Brass texture.

Phase discrimination

EBSD can be used to discriminate crystallographically dissimilar phases by comparing the interplanar angles measured from the diffraction pattern, with calculated angles from a set of candidate phases, and selecting the best fit. Figure 21 shows the separation of the austenite and ferrite phases in a duplex stainless steel. Austenite is face centered cubic, and ferrite is body centered cubic, and the phases can not be distinguished by X-ray microanalysis. The phase map shows that 38.6% of the sampled area is ferrite and 60.7% is austenite. The crystal orientation maps also reveal the constituent grains in the two phases.

Figure 21: Illustration of phase discrimination in a sample of duplex stainless steel. The map step size is 0.45 µm and contains 49152 points.

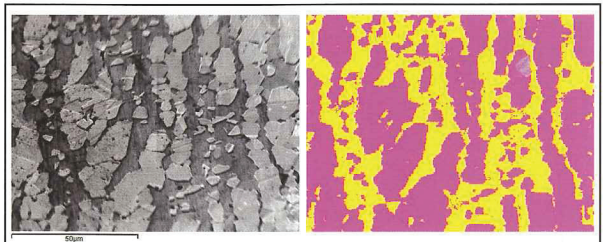

Electron image

Map showing separation of the two phases. Ferrite is yellow, austenite is purple

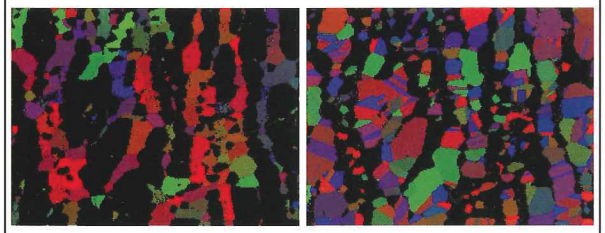

Normal direction crystal orientation map from ferrite phase

Normal direction crystal orientation map from austenite phase

Summary

- A crystal orientation map can be acquired by scanning the electron beam over a sample and analyzing the diffraction pattern formed at each point.
- Crystal orientation maps definitively reveal the sample microstructure and can measure grain size distributions, grain boundary misorientations and special boundaries and show their location in the sample.
- The individual crystal orientation measurements can be displayed to show crystallographic texture or preferred orientation. Texture components can be separated and the regions of the sample contributing to those components shown.
- EBSD can also be used to distinguish crystallographically different phases and to show their location, abundance and preferred orientations.

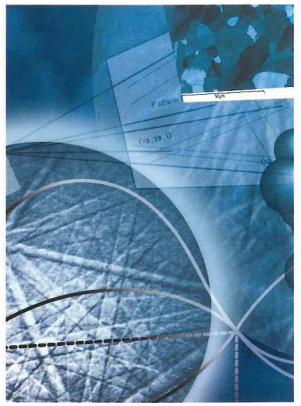

Section 3

Undertaking EBSD experiments

Sample preparation

EBSD is very sensitive to crystalline perfection, and sample preparation may be needed to remove any surface damage. A well prepared sample is a prerequisite to obtaining a good diffraction pattern. Surfaces must be sufficiently smooth to avoid forming shadows on the diffraction pattern from other parts of the sample. Suitable techniques for use with EBSD include:

- For metals and insulators: mounting in conductive resin, mechanical grinding, diamond polishing and final polishing with colloidal silica.
- For metals: mounting in conductive resin, mechanical grinding, diamond polishing and electropolishing.
- Brittle materials such as ceramics and geological materials can often be fractured to reveal surfaces immediately suitable for EBSD.
- Ion milling for materials which are not amenable to conventional metallography such as zirconium and zircalloy.
- Dual focused ion beam – electron beam microscopes fitted with EBSD can perform in-situ specimen preparation for EBSD.
- Plasma etching for microelectronic devices.

Charging in non-conductive samples can be eliminated, as for X-ray microanalysis, by the deposition of a conducting layer. The deposited layer must be very thin – for example 2 to 3 nm of carbon or gold/palladium – otherwise a diffraction pattern will not be obtained. It may be necessary to increase the electron accelerating voltage to penetrate the conducting layer.

Charging can be reduced when the sample is tilted for EBSD experiments and can also be reduced by analyzing the sample in an environmental or low vacuum SEM.

Camera integration time and resolution

Because the luminous intensity of the diffraction pattern on the phosphor screen is low, using a short integration time on the CCD camera may give a poor signal to noise ratio. In this case, integrating for longer on the CCD will improve the visibility of the diffraction pattern (Figure 22). The camera may be cooled to reduce electronic noise in the CCD when used in this way. The yield of back scattered electrons increases with atomic number, so low atomic number materials will require a longer integration time than higher atomic numbers.

The CCD camera resolution can also effect the integration time required to collect a diffraction pattern. Current CCD cameras can collect 12 bit images at a resolution of 1300 x 1024 pixels. Using "pixel binning", neighboring pixels in the CCD can be added together to form a single pixel in the image. When pixels are binned in this way, less integration time is required to achieve a given signal in the image pixel because the detecting pixel area is larger. For example, if a satisfactory diffraction pattern is obtained in 12 ms at 1300 x1024 resolution, a comparable pattern can be obtained in 3 ms at 650 x 512 resolution.

It is not essential to collect high resolution diffraction patterns for crystal orientation mapping, because the Hough transform always operates on a 128 x128 resolution image. In addition, the transform works well on noisy images (Figure 23) so some experimentation is necessary to determine the optimum integration time required when collecting maps.

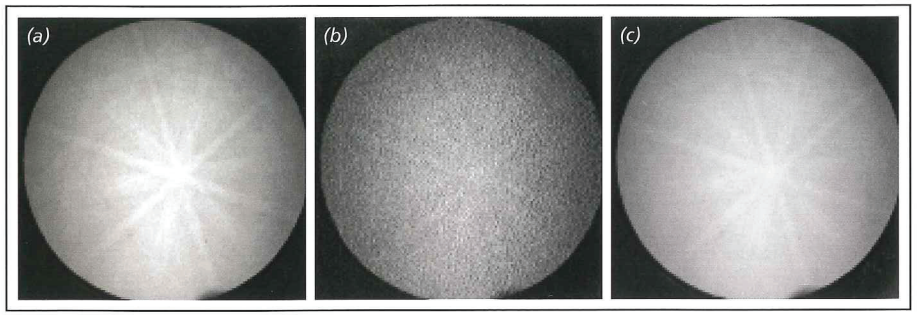

Figure 22: Effect of integration time and probe current on diffraction pattern. (a) 36 ms, 2 nA. (b) 36 ms 200 pA, (c) 360 ms 200 pA. (Probe currents are approximate)

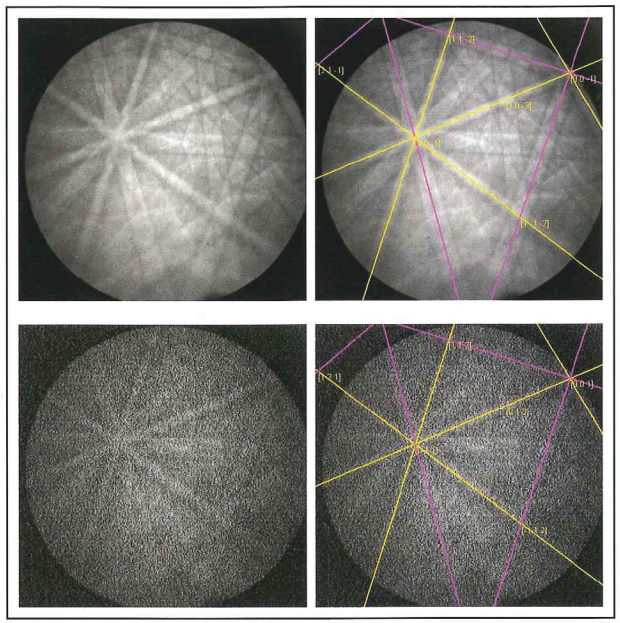

Figure 23: Diffraction patterns can be automatically solved in the presence of noise.

Background removal

Electrons of all energies scattered from the sample form a background to the diffraction pattern, which reduces the contrast of the Kikuchi bands. The background intensity can be removed to improve the visibility of the Kikuchi bands. The background can be measured by scanning the beam over many grains in the sample to average out the diffraction information. The background can be removed by subtraction from, or division into, the original pattern. (Figure 24)

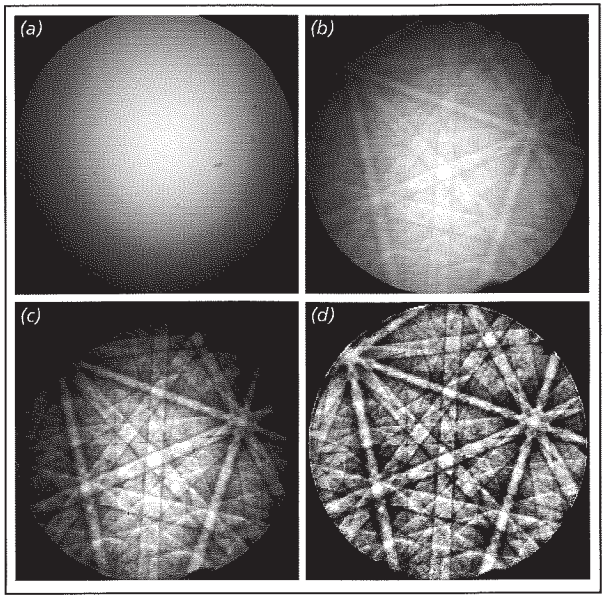

Figure 24: Background removal from diffraction pattern of iron. (a) Background (b) Original pattern (c) Background subtraction (d) Background division.

Microscope operating conditions

It is very important to understand the effect of varying the microscope operating conditions on the diffraction pattern.

Probe current

Increasing the probe current will increase the number of electrons contributing to the diffraction pattern and so allow the camera integration time to be reduced (Figure 22). However, this must be balanced with the spatial resolution required, because increasing the probe current will also increase the electron beam size.

Accelerating voltage

Increasing the accelerating voltage reduces the electron wavelength and hence reduces the width of the Kikuchi bands in the diffraction pattern (see equation 2). Also, because more energy is being deposited on the phosphor screen, this will result in a brighter pattern which requires a shorter integration time (Figure 25). Changing the accelerating voltage may require adjustment to the Hough transform filter size to ensure the Kikuchi bands are detected correctly. Higher accelerating voltages may be required to penetrate conducting layers, and lower accelerating voltages for restraining the beam to thin layers, or for charging samples.

Working distance and magnification

Because the sample is tilted, the SEM working distance will change as the beam position moves up or down the sample, and the image will go out of focus (Figure 5). The image will also be foreshortened because of the tilt, and at low magnifications much of the field of view could be out of focus. Some EBSD systems can compensate for the image foreshortening by using different horizontal and vertical image beam steps, and can adjust the SEM focus automatically as the beam is moved over the sample (Figure 26).

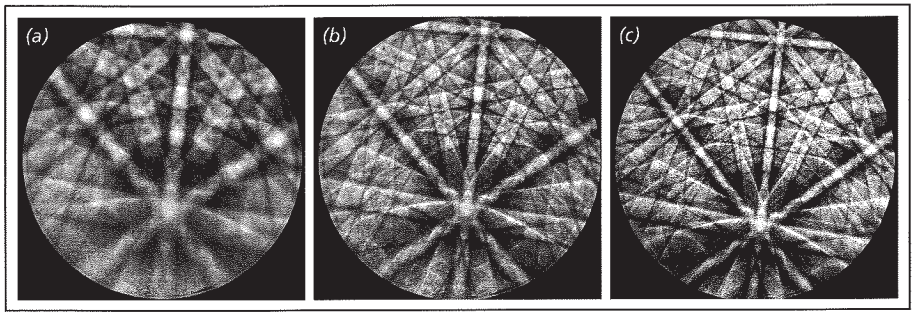

Figure 25: Effect of changing accelerating voltage on diffraction patterns from nickel. Note that there is an effect on the bandwidth, sharpness and contrast. (a) 10kV, (b) 20 kV, (c) 30kV

Figure 26: Tilt correction and focus maintenance.

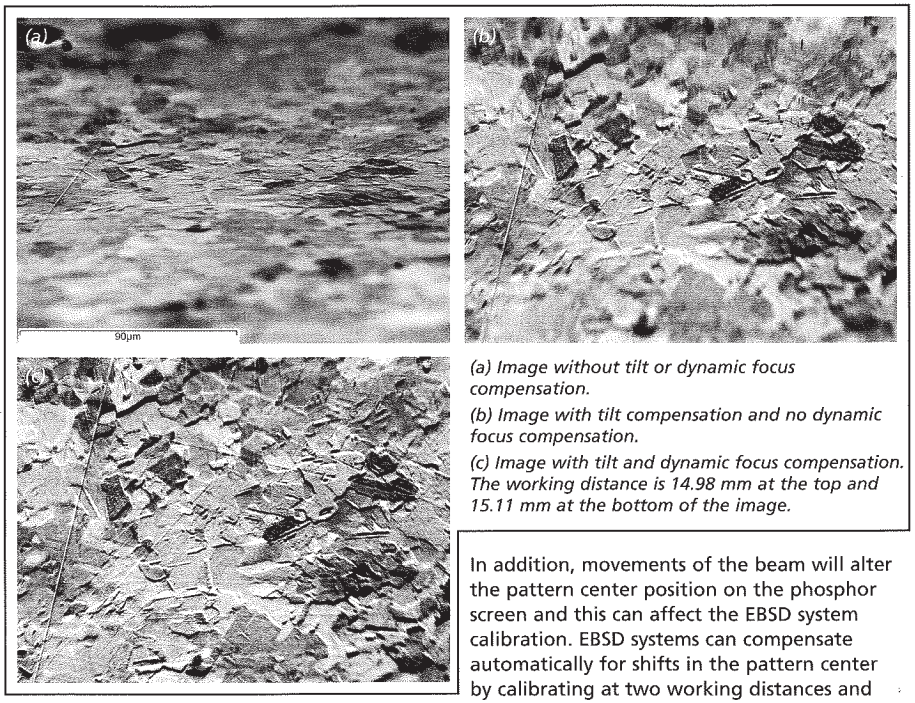

(a) Image without tilt or dynamic focus compensation.

(b) Image with tilt compensation and no dynamic focus compensation.

(c) Image with tilt and dynamic focus compensation. The working distance is 14.98 mm at the top and 15.11 mm at the bottom of the image.

In addition, movements of the beam will alter the pattern center position on the phosphor screen and this can affect the EBSD system calibration. EBSD systems can compensate automatically for shifts in the pattern center by calibrating at two working distances and interpolating for intermediate working distance values. It is important to know the range of working distances for which the EBSD system will remain accurately calibrated.

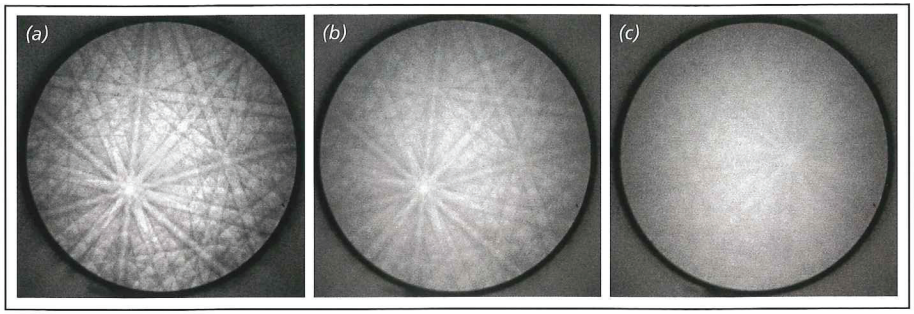

Figure 27: Effect of SEM vacuum on diffraction pattern from platinum sample (a) 0.05 torr (b) 0.5 torr (c) 1.0 torr

Pressure

Diffraction patterns can also be collected from samples at low vacuum in environmental SEMs (Figure 27). This can be useful with specimens which may otherwise charge, such as ceramic or geological materials.

Effect of sample tilt

The EBSD sample is usually tilted at 70° to the horizontal to optimize both the contrast in the diffraction pattern and the fraction of electrons scattered from the sample. For smaller tilt angles the contrast in the diffraction pattern decreases (Figure 28).

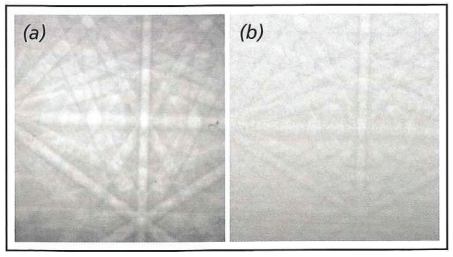

Figure 28: Diffraction patterns from germanium at 20 kV. (a) 70° sample tilt (b) 50° sample tilt

Spatial resolution

The electrons contributing to the diffraction pattern originate within nanometres of the sample surface. Hence, the spatial resolution will be related to the electron beam diameter, and this depends on the type of electron source and probe current used. Typical beam diameters at 0.1 nA probe current and 20 kV accelerating voltage are 2 nm for a FEG source, and 30 nm for a tungsten source. The beam profile on the sample surface will also be elongated in the direction perpendicular to the tilt. The spatial resolution achieved in practice will depend on the sample, SEM operating conditions and electron source used, and under optimum conditions, grains as small as 10 nm can be identified.

Measurement accuracy

Orientation measurement

Errors in crystal orientation measurements from the diffraction pattern will depend principally on the accuracy of the Kikuchi band position measurement and the system calibration, and are generally in the range ±0.5°. To avoid systematic errors in orientation measurements made with respect to the sample axes for texture measurements, care should be taken to ensure that the sample normal and longitudinal directions are oriented correctly with respect to the phosphor screen.

Residual errors

For each orientation measurement a residual angle θ_ε can be calculated where

$$\theta_\varepsilon = \sqrt{\sum_{i=1\text{-}n} (\theta_i^m - \theta_i^c)^2} \qquad (6)$$

θ_i^m is the measured angle between the ith pair of Kikuchi bands, θ_i^c is the actual angle between the corresponding crystal planes and n is the number of Kikuchi band pairs. θ_ε is a measure of the degree of fit of a solution to the diffraction pattern and is used to rank possible solutions. Residual error values higher than 1.5° can suggest the system calibration needs to be checked.

Summary

- Careful sample preparation is critical for successful EBSD experiments, and conventional metallographic techniques can normally be used successfully.
- It is important to balance the requirements of total experiment time, orientation accuracy and spatial resolution when designing an EBSD experiment.
- The orientation measurement accuracy is typically ±0.5°.
- The spatial resolution of EBSD depends on the sample, microscope type and microscope operating conditions and in a FEGSEM, grains as small as 10 nm can be analyzed.

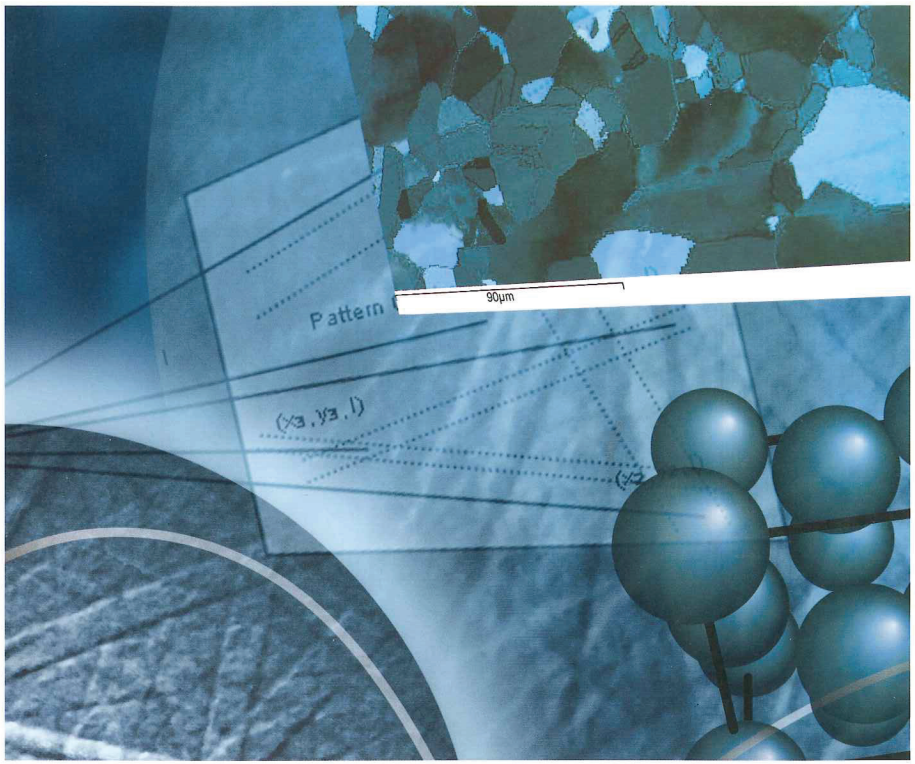

Section 4

Basic crystallography for EBSD

Crystals and lattices

Crystalline material consists of a regular repetition of a group of atoms in three dimensional space.

A crystal lattice is an infinitely repeating array of points in space (Figure 29). The unit cell of the lattice is the basic repeating unit of the lattice, and is characterized by a parallelepiped with cell edge lengths a, b, c and inter axis angles α, β, γ (Figure 30). These unit cells can be classified as belonging to one of fourteen Bravais lattices. Each Bravais lattice belongs to one of the seven crystal systems. (Figure 31). The motif is the group of atoms repeated at each lattice point, which generates the crystalline structure of the material (Figure 32).

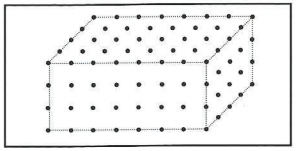

Figure 29: A crystal lattice

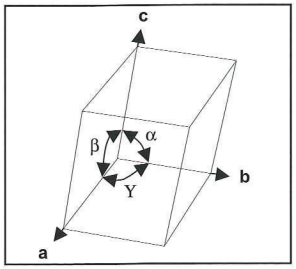

Figure 30: Unit cell of a lattice

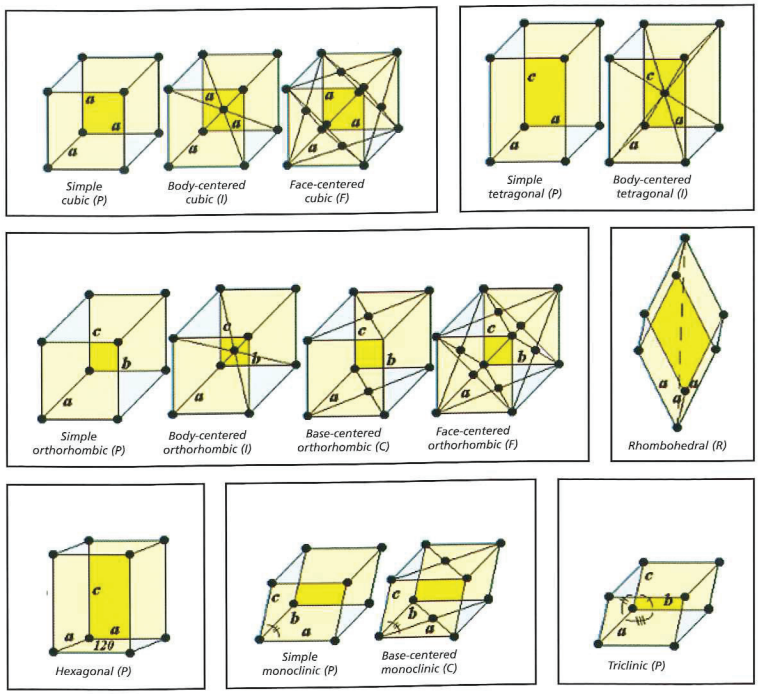

Figure 31: The fourteen Bravais lattices. Each Bravais lattice belongs to one of the seven crystal systems: cubic, tetragonal, orthorhombic, rhombohedral, hexagonal, monoclinic and triclinic. P = primitive, I = body centered, F = face centered, C = base centered.

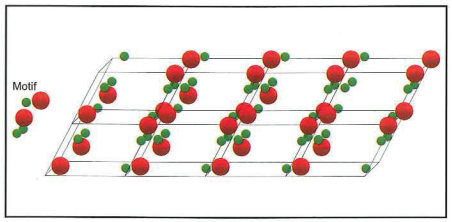

Figure 32: Crystal structure showing a repeated atomic motif at each lattice point

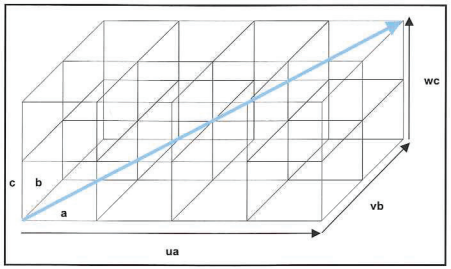

Figure 33: Meaning of the crystal direction [uvw]. The direction shown here is [422]

Crystal directions, planes and the zone axis

Consider a crystal lattice with unit cell edges a, b and c (Figure 30). A crystal direction [uvw] is parallel to the direction joining the origin of the crystal lattice with the point with coordinates (ua, vb, wc) (Figure 33).

A plane with Miller indices (hkl) passes through the three points (a/h,0,0), (0, b/k,0) and (0,0, c/l) on the edges of the unit cell. The set of parallel lattice planes passes through all similar points in the lattice. The plane d-spacing is the perpendicular distance from the origin to the closest plane and also the perpendicular distance between successive planes. (Figure 34). In materials with cubic symmetry the crystal direction [uvw] and the normal to the plane (uvw) are parallel.

The common direction shared by two crystal planes when they intersect is called the zone axis (Figure 35). A zone axis [uvw] is always perpendicular to the plane normal (hkl) that comprises the zone, and this relation is stated in the zone law: $uh + vk + wl = 0$.

The family of symmetrically related directions [uvw] is shown by the notation <uvw> and the family of symmetrically related planes (hkl) is shown by the notation {hkl}.

Figure 34: Crystal planes

(a) The plane with Miller indices (hkl) makes intercepts a/h, b/k and c/l on the edges of the unit cell. The plane shown here is (221) because the intercept in the a direction is 1/2a, in the b direction 1/2b and in the c direction c.

(b) A set of parallel (221) planes intersecting the edges of the unit cells. The d-spacing for these planes is the perpendicular distance between successive planes or equivalently the perpendicular distance from the origin to the closest plane.

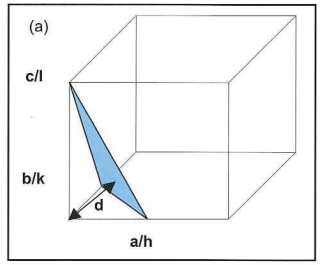

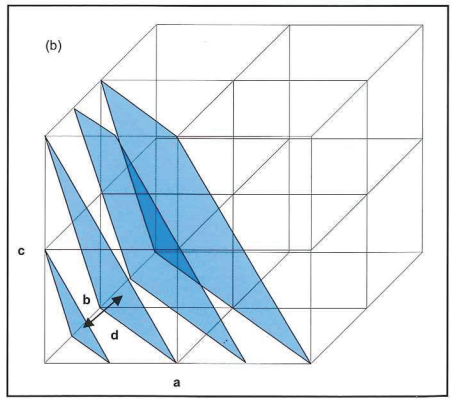

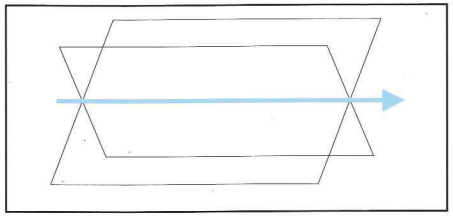

Figure 35: The zone axis is the common crystal direction shared by two planes

Crystal orientation

A crystal orientation is measured with respect to an orthogonal coordinate system fixed in the sample. The sample system is normally aligned with directions used in texture measurements on rolled sheet materials. The x axis is parallel to the rolling direction of the sample (RD), the y axis parallel to the transverse direction (TD) and the z axis parallel to the normal direction (ND) (Figure 36).

The relationship between a crystal coordinate system and the sample system is described by an orientation matrix G. A direction measured in the crystal system $\mathbf{r}_c$ is related to the same direction measured in the sample system $\mathbf{r}_s$ by:

$$\mathbf{r}_c = \mathrm{G}\mathbf{r}_s$$

The rows of the matrix G are the direction cosines of the crystal system axes in the coordinates of the sample system.

$$\mathrm{G} = \begin{pmatrix} \cos\alpha_1 & \cos\beta_1 & \cos\gamma_1 \\ \cos\alpha_2 & \cos\beta_2 & \cos\gamma_2 \\ \cos\alpha_3 & \cos\beta_3 & \cos\gamma_3 \end{pmatrix}$$

Figure 36 shows how the angles α_1, β_1, γ_1, are defined. α_2, β_2, γ_2 and α_3, β_3, γ_3 are similarly defined as the angles between the [010] and [001] crystal directions and the three sample axes.

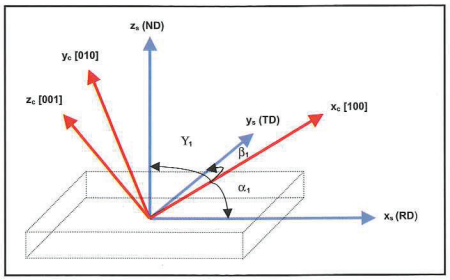

Figure 36: Relationship between crystal and sample coordinate systems. α_1, β_1 and γ_1 are the angles between the crystal direction [100] and RD, TD and ND respectively.

Misorientation

The orientation between two crystal coordinate systems can also be defined by the angle-axis pair θ[uvw].
One coordinate system can be superimposed onto the other by rotating by an angle θ around the common axis [uvw] (Figure 37). Because it is an axis of rotation, the direction [uvw] is the same in both coordinate systems. The angle-axis pair notation is normally used to describe grain boundary misorientations (see box 3).

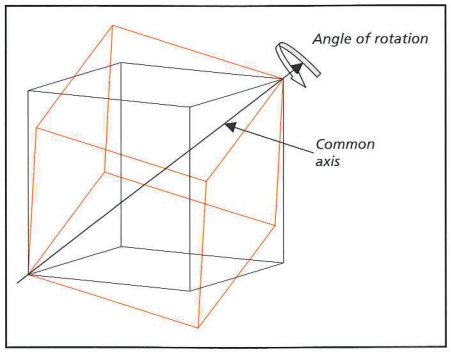

Figure 37: Two interpenetrating lattices can be realigned by a single rotation about a common axis [uvw] by an angle θ. In the figure the axis is the common [111] direction and the rotation angle 60°.

Euler angles

The orientation between two coordinate systems can also be defined by a set of three successive rotations about specified axes. These rotations are called the Euler angles $\varphi_1 \Phi \varphi_2$ and are shown in Figure 38.

(hkl)[uvw]

A crystal orientation is also represented by a crystal direction [uvw] that is parallel to the rolling direction of the sample, and the crystal plane normal (hkl) that is parallel to the sample normal.
(See Figure 10)

Stereographic projections

Directions can be represented in two dimensions with a stereographic projection (Figure 39). Consider a sphere with centre O, south pole S and a point P on its surface. The line SP intersects the equatorial plane at p. Hence, any direction OP can be represented by a corresponding stereographic projection point p on the equatorial plane.

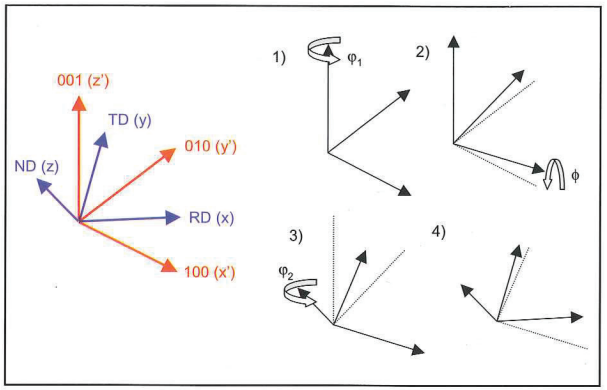

Figure 38: Definition of the Euler angles $\varphi_1 \Phi \varphi_2$. This shows the rotations necessary to superimpose the crystal coordinate system (red) onto the sample system (blue). The first rotation φ_1 is about the z axis of the crystal coordinate system. The second rotation is Φ about the new x-axis. The third rotation is φ_2 about the new z-axis. The dotted lines show the positions of the axis before the last rotation. Note that the orientation can also be defined by an equivalent set of Euler angles which superimpose the sample coordinate system onto the crystal coordinate system.

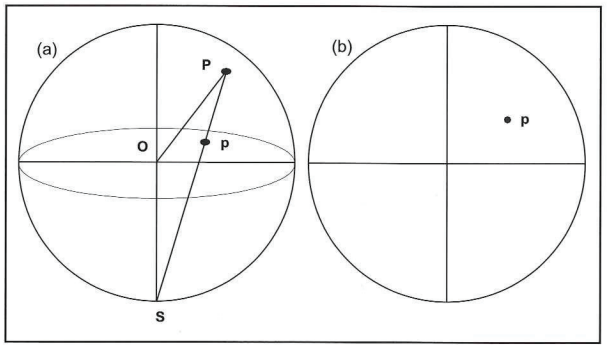

Figure 39: The stereographic projection.
(a) Projection of a point P on the surface of a sphere with centre O from the projection point S onto the equatorial plane at p.
(b) The stereographic projection is the equatorial plane of this sphere with the point p representing the direction OP.

For texture studies of rolled materials, the axes of the projection sphere can be aligned with the axes of the sample. The sample normal is the center of the projection and the rolling direction chosen to be at the right of the projection. If a unit cell with cubic symmetry is placed at the center of the projection sphere, then the crystal directions and plane normals can be projected onto the equatorial plane and the directions represented as a stereographic projection (Figure 40).

In an inverse pole figure the crystallographic directions parallel to particular directions in the sample are plotted on a stereographic projection (Figure 41).

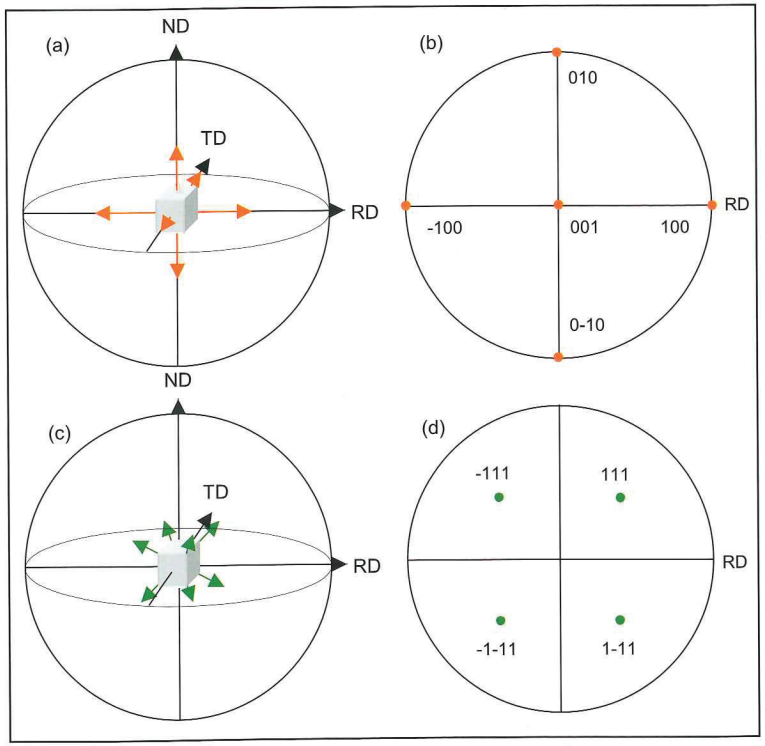

Figure 40: Stereographic projections of a cubic unit cell with edges parallel to RD, ND and TD. The orientation is (001)[100]

(a) The six {001} plane normals (poles) are shown.

(b) A stereographic projection of these directions. (Directions that project beneath the equatorial plane are not shown.) This is a (100) pole figure of this crystal orientation.

(c) The eight {111} plane normals are shown.

(d) A stereographic projection of these directions which is a (111) pole figure of this crystal orientation.

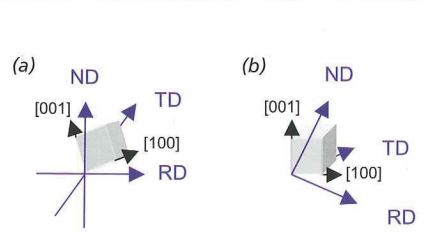

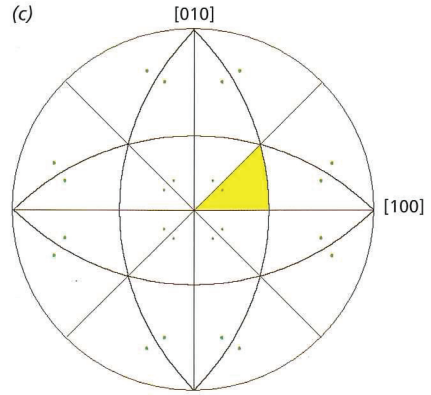

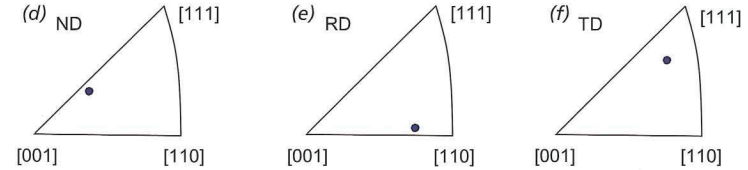

Figure 41: Formation of an inverse pole figure

(a) A cubic crystal unit cell oriented with respect to the sample axes.

(b) The same sample axes oriented with respect to the crystal unit cell.

(c) The crystallographic direction parallel to ND plotted on a stereographic projection with axes parallel to the edges of the crystal unit cell. The direction is repeated because, for cubic materials, it could be anyone of 48 symmetrically equivalent crystal directions.

(d) The yellow area from the stereographic projection in (c) is extracted to form the ND inverse pole figure. Only one stereographic triangle is required for this projection because the other triangles in the projection are symmetrically equivalent.

(e) and (f)
The RD and TD inverse pole figures are obtained in a similar way.